Human Biodistribution and Radiation Dosimetry of the Tachykinin NK_1 Antagonist Radioligand [^{18}F]SPA-RQ: Comparison of Thin -Slice, Bisected, and 2-D Planar Image Analysis

David R. Sprague, BA[1]; Frederick T. Chin, PhD[1,*]; Jeih-San Liow, PhD[1]; Masahiro Fujita, MD, PhD[1]; H. Donald Burns, PhD[2]; Richard Hargreaves, PhD[2]; James B. Stubbs, PhD[3]; Victor W. Pike, PhD[1]; Robert B. Innis, MD, PhD[1]; P. David Mozley, MD[2]

[1] Molecular Imaging Branch, NIMH, National Institutes of Health, Bethesda, MD, USA
[2] Merck Research Laboratories, West Point, PA, USA
[3] Radiation Dosimetry Systems, Inc., San Francisco, CA, USA

[*] Present affiliation: Stanford University School of Medicine, Stanford, CA, USA

For correspondence or reprints contact:

Robert B. Innis, MD, PhD, Chief of Molecular Imaging Branch
Molecular Imaging Branch, NIMH
National Institutes of Health
Bldg. 1, Rm. B3-11, 1 Center Drive, MSC 0135
Bethesda, MD 20892-0135
Tel: 301-594-1368
Fax: 301-480-3610
Email: robert.innis@nih.gov

First Author's contact information:

David R. Sprague, BA, Postbaccalaureate Intramural Research Training Award Fellow
Molecular Imaging Branch, NIMH
National Institutes of Health
Bldg. 1, Rm. B3-10, 1 Center Drive, MSC 0135
Bethesda, MD 20892-0135
Tel: 301-594-1089
Fax: 301-480-3610
Email: dsprague12@aol.com

Word Count: 4,339 words

Running foot line: Dosimetry of [^{18}F]SPA-RQ

ABSTRACT

Purpose: ^{18}F-Labeled Substance P Antagonist-Receptor Quantifier ([^{18}F]SPA-RQ) is a selective radioligand for *in vivo* quantification of tachykinin NK_1 receptors with positron emission tomography (PET). The aims of this study were to estimate the radiation burden of [^{18}F]SPA-RQ based on human whole-body PET imaging and to compare three methods of image analysis. **Methods**: Whole-body PET images were acquired in seven healthy subjects following injection of 192 ± 7 MBq (5.2 ± 0.2 mCi) [^{18}F]SPA-RQ. Emission images were acquired from 0–120 and 180–240 min post-injection. Urine samples were collected at three time points to measure excreted radioactivity. Horizontal tomographic images were compressed to varying degrees in the anteroposterior direction to create three data sets: thin-slice, bisected, and 2-D planar images. Regions of interest were drawn around visually identifiable source organs to generate time-activity curves for each data set. Residence times were determined from these curves, and doses to individual organs and the body as a whole were calculated using OLINDA/EXM 1.0. **Results**: The lungs, upper large intestine wall, small intestine, urinary bladder wall, kidneys, and thyroid had the highest radiation-absorbed doses. Biexponential fitting of mean bladder and urine activity showed that about 41% of injected activity was excreted via urine. Assuming a 2.4 h urine voiding interval, the calculated effective doses from thin-slice, bisected, and 2-D planar images were 29.5, 29.3, and 32.3 µSv/MBq (109.0, 108.3, and 119.6 mrem/mCi), respectively. **Conclusions**: Insofar as effective dose is an accurate measure of radiation risk, all three methods of analysis provided quite similar estimates of risk to human subjects. The radiation dose was moderate and would potentially allow subjects to receive multiple PET scans in a single year. Individual

organ exposures varied among the three methods, especially for structures asymmetrically located in an anterior or posterior position. Bisected and 2-D planar images almost always provided more conservative organ dose estimates than thin-slice images. Thus, either the bisected or 2-D planar method of analysis appears acceptable for quantifying human radiation burden, at least for radioligands with a relatively broad distribution in the body, and not concentrated in a small number of radiation sensitive organs.

Key Words: [^{18}F]SPA-RQ, positron emission tomography, dosimetry, biodistribution

INTRODUCTION

The neuropeptide Substance P (SP) and its preferred receptor, the tachykinin NK_1 receptor, are widespread throughout the mammalian nervous system (*1*). Substance P has been proposed to play a role in a number of neurological and psychiatric diseases, as well as chemically induced nausea and vomiting (*2-10*). However, to date, NK_1 receptor antagonists have only found proven efficacy in the prevention of acute and delayed chemotherapy induced nausea and vomiting (*2*) despite extensive pre-clinical and clinical work suggesting utility in pain, anxiety, depression, schizophrenia, Rett's Syndrome, Parkinson's disease and Alzheimer's disease (*3-10*). The widespread distribution of central SP pathways and NK_1 receptors in the human brain *in vivo* is a paradox given the apparent lack of effect of drugs designed to block these systems in so many central disorders. Detailed study of these systems in health and neurological disease is an important topic for research since it may identify opportunities for future clinical trials with NK_1 receptor antagonists.

^{18}F-Labeled Substance P Antagonist-Receptor Quanitifier ([^{18}F]SPA-RQ) [2-fluoromethoxy-5-(5-trifluoromethyl-tetrazol-1-yl)benzyl]-[(2S, 3S)-2-phenyl-piperidin-3-yl)-amine is a highly selective radiopharmaceutical with a subnanomolar affinity for the human NK1 receptor in vitro. It has been used previously in guinea pig, monkey and human PET studies (*11-12*). In these studies, [^{18}F]SPA-RQ demonstrated high brain uptake, displacement by NK_1 selective ligands and low nonspecific binding. The absence of receptors in the cerebellum seems to facilitate quantification. The principal purpose of the present study was to determine the human whole-body biodistribution of [^{18}F]SPA-

RQ and to estimate radiation absorbed doses of individual organs. The effective dose (ED) was calculated as the primary surrogate of radiation safety.

Modern PET cameras map the distribution of radioactivity in 3-dimensional (3D) volumes. These volumes can be parsed into tomographic slices and reinterpolated for analysis in any plane. The thickness of each tomographic slice is under the control of the imager. While most PET scans are reformatted to produce slice thicknesses that vary from a few millimeters to about a centimeter, it is possible to compress all of the slices into a single, 2D image that looks much like a planar scintigram. Previous work conducted by our laboratory indicated that dosimetry analyses performed on single compressed planar images as opposed to multiple tomographic images were considerably less time consuming and provided only slightly higher (*i.e.*, more conservative) values of estimated radiation doses (*13*). Thus, the second aim of the present study was to determine the efficacy and efficiency of using either a compressed 2-D planar image or anteroposterior-bisected images instead of thin-slice images for the analysis of human whole-body dosimetry studies.

MATERIALS AND METHODS

Subjects

The Radiation Safety Committee of the National Institutes of Health (NIH) and the Institutional Review Board of the National Institute of Mental Health (NIMH) approved the use of [^{18}F]SPA-RQ in human subjects for this study. Four male and three female healthy volunteers (age, 28 ± 7 y; range, 23–40 y; weight, 77 ± 5 kg) participated in the protocol. These and subsequent data are expressed as the mean ± SD unless

otherwise noted. Subjects gave informed, written consent and then completed a screening assessment no more than three months prior to their PET scan. The assessment included a history, physical examination, electrocardiogram (ECG), and standard blood and urine analyses to ensure that subjects were free of any medical or neuropsychiatric illnesses. The laboratory tests included a complete blood count, serum chemistries, thyroid function test, urinalysis, urine drug screen, as well as syphilis, HIV and hepatitis B screenings. Approximately 24 h after the administration of the tracer, subjects returned to repeat the complete blood count, serum chemistries and urinalysis.

Radiopharmaceutical Preparation

The chemical precursor, (2S-cis)-3-[[[2-hydroxy-5[5-(trifluoromethyl)-1H-tetrazol-1-yl]phenyl]methyl]amino]-2-phenyl-1-piperidinecarboxylic acid 1,1,-dimethylethyl eter, was obtained from Merck Research Laboratories, and the radioligand, [^{18}F]SPA-RQ, was prepared according to the route and method originally described by Solin *et al*. (*11*), but with significant modifications as described by Chin *et al*. (*14*). For the present study, the radiochemical purities of all syntheses of [^{18}F]SPA-RQ were > 99% with an average specific activity of 46.6 ± 16.6 GBq/μmol (1.26 ± 0.45 Ci/μmol) at the time of injection.

PET Data Acquisition

Both a pre-injection transmission scan and a series of dynamic emission scans were acquired using a GE Advance tomograph (GE Medical Systems, WI). The PET device was calibrated daily with a ^{137}Cs source and cross-calibrated weekly to a well counter using a known amount of ^{18}F activity contained in a 16-cm diameter, cylindrical phantom. Each subject was imaged in seven contiguous 15-cm segments from the top of

the head to a point below the gonads that varied depending on the height of the subject. To minimize extraneous motion, all subjects wore a mask that affixed their head in a single position and had their arms and abdomen wrapped with body-restraining sheets. Blood pressure, pulse, and respiration rates were obtained prior to the administration of [^{18}F]SPA-RQ and at three time points during the emission scans.

Before injection of the radioligand, a 21 min transmission scan (3 min at each of the 7 body segments) using rotating ^{68}Ge rods was acquired for subsequent attenuation correction. Then, an initial set of dynamic emission scans consisting of 14 cycles was acquired following the intravenous injection of 192 ± 7 MBq (5.2 ± 0.2 mCi) [^{18}F]SPA-RQ. The acquisition of each cycle began with an emission scan at the first bed position (*i.e.*, the head), and continued by moving the bed distally to the next body segment for a total of seven segments. The scan of the seventh segment completed a cycle, and the bed was moved back to the original position. The length of time that each segment was imaged within each of the 14 cycles varied as follows: 4 x 0.25, 3 x 0.5, 3 x 1, 3 x 2 and 1 x 4 min. The 6 movements of the bed between segments 1 through 7 required 3 s each, and the repositioning of the bed following the completion of each of the cycles required 13 s. Thus, the total length of the initial emission scan was about 120 min.

Following the completion of the first emission scan, the subjects were allowed to rest for about 30 min. During this time, all voided urine was collected for measurement of radioactivity. The subject then returned to the scanner and was positioned in, and affixed to, the same approximate location on the bed as for the first scan. A second 21 min transmission scan, identical to the first, was performed followed by a second set of dynamic emission scans that began about 3 h after injection of radioligand. The emission

scan consisted of 2 cycles with segment imaging times of 4 min each for a total scan time of about 60 min. After completing all scans, the subject was asked to void before leaving NIH so the activity in urine could be measured. The subject went home with a 24-h urine collection container, and we measured urine radioactivity the next day. Radioactivity was measured with a gamma counter that was cross-calibrated with the GE Advance scanner.

Image Analysis

The 256 original tomographic PET slices were compressed in the anteroposterior (*i.e.*, coronal) direction to create three whole-body image groups: thin-slice, bisected, and 2-D planar. Sets of six contiguous tomographic slices were compressed for the thin-slice image set and had a thickness of about 1.2 cm. Two sets of 128 tomographic slices were compressed for the bisected images. In effect, this roughly divided the body through the coronal midline into anterior and posterior sections to create two horizontal planar images. The 2-D planar images contained all 256 tomographic slices compressed into a single coronal image. All three sets of images were analyzed using PMOD 2.61 (pixel-wise modeling computer software, PMOD group, Zurich, Switzerland).

The brain, thyroid, heart, right lung, right kidney, liver, and testes were all identifiable as source organs on the thin-slice images. Regions of interest (ROIs) were carefully drawn around each of these structures on each of the slices in which they appeared, and these ROIs were propagated across all 16 acquisition time points. The right lung was selected to avoid the heart, and total activity in the lungs was calculated assuming that the right lung would account for 55% of total uptake (*15*). Though the right kidney partially overlapped the liver, it was easier to identify on the images than the left

kidney, which was often occluded by diffuse activity in the abdominal cavity and the spleen. Total uptake of activity in the kidneys was calculated as twice that of the right kidney.

In addition to the previously mentioned source organs, the intestines, urinary bladder and red marrow showed moderate levels of [^{18}F]SPA-RQ uptake. A region of interest (ROI) was drawn around the entire area enclosed by the lateral abdominal walls from the inferior borders of the liver and diaphragm to the superior dome of the urinary bladder. After subtracting the activity in kidneys from the total activity encompassed by this large ROI, the remainder was assigned to the intestines. Individual ROIs were drawn around the urinary bladder at each time point to account for the changing size of the bladder as it accumulated urine. The activity in these separate urinary bladder ROIs was then summed to represent total bladder uptake. [^{18}F]SPA-RQ exhibited very low levels of defluorination in human subjects; only marrow-rich bone structures (e.*g.*, vertebrae, pelvis, and skull) exhibited uptake of the radioligand. In contrast, the marrow-poor diaphyses of tubular bones were not visible. Thus, all bone-related uptake of the tracer was assumed to derive from red marrow. This uptake was quantified by drawing a horseshoe-shaped ROI around the superior and lateral aspects of the skull. Total red marrow uptake was calculated by conservatively estimating that the skull accounted for 8% of all red marrow uptake (*15*).

All of the above organs were identified and assigned ROIs on both the bisected and 2-D planar images. If an organ appeared in both the anterior and posterior slices of the bisected images, ROIs were drawn around the structure on both slices. For both the bisected and 2-D planar image analyses, large ROIs were drawn surrounding each source

organ to ensure that all accumulated radioactivity within a particular organ was included. Although the heart, testes and thyroid were not always as clearly visible as the other source organs on the bisected and 2-D planar images, the regions could still be drawn with moderate confidence using other structures as anatomical landmarks. The inclusion of the testes and, to a lesser extent, the thyroid and red marrow as source organs was significant because of their sensitivity to radiation and relatively high weighting factors in the calculation of the overall ED. For all three image sets, the activity in the "remainder of the body" was calculated as the residual activity from the sum of the midpoint time measurements of all source organs.

Residence Time Calculation

The non-decay-corrected activity from each source organ, with the exception of the urinary bladder and the intestines, was converted to a percentage of the injected activity (IA). A time–activity curve was created for each organ by plotting the percentage of IA versus time. The area under an organ's activity curve from time zero to infinity is equal to residence time. The trapezoidal rule was used to calculate the area under the curve from the time of injection to the time image acquisition terminated. Any further decline in activity was assumed to occur only through physical decay without any biological clearance.

Many of the source organs were not confined to a single 15-cm bed position, resulting in multiple acquisition time points for single organs. In these cases, new time points were generated before creating the organ's activity curve. A more accurate mean acquisition time for affected organs was obtained by averaging the time points associated with each bed position in which the organ appeared.

The residence time of the urinary bladder was determined using the dynamic bladder model (*16*) in OLINDA/EXM 1.0 (Organ Level Internal Dose Assessment/Exponential Modeling computer software, Vanderbilt University, 2003) (*17*). Voiding intervals of 0.6, 1.2, 2.4 and 4.8 h were used to calculate several different residence times to determine their effect on dose to urinary bladder wall. Because subjects were allowed to urinate between the two emission scans, activity in the urinary bladder ROIs had to be corrected for excretion. Total urine excretion during the first scanning session of about 2h was equal to the amount of activity in the urinary bladder ROIs. Summing the activity contained in the urine collected during the break between the two emission scans with the activity found in the urinary bladder ROIs during the second emission scan provided values for total urine excretion up to about 4 h after injection. Finally, the urine activities from the 2-, 4- and 24-h post-injection urine collections were summed for each subject to provide a final value for total urine excretion. A cumulative urine activity curve was generated for each subject and fitted with a biexponential curve to determine of total urine excretion as a fraction of IA. The formula for the biexponential curve was: $y = a_1(1-e^{-\lambda t}) + a_2(1-e^{-\gamma t})$, where y is total urine excretion as a fraction of IA, $a_1 + a_2$ equals the total measured urine excretion as a fraction of IA, λ and γ are the two exponential rate constants, and t equals time. The sum of the two intercepts was restricted to values between 0 and 1: $0 > a_1 + a_2 < 1$.The total urine excretion as a fraction of IA was converted into an ED for the urinary bladder wall in OLINDA/EXM 1.0.

One subject failed to return her 24-h urine collection; total urinary excretion for this person was calculated as the average of the other subjects. A second subject's 2- and

4-h post-injection urine collections demonstrated activities that were inconsistent with the data obtained from the PET images. This discrepancy was assigned to an error in the gamma counter used to measure the activity of the urine. Two- and 4-h urine activities were determined for this subject by assuming that he/she was able to void the entire amount of activity accounted for in the urinary bladder ROIs at the final time points of the first and second emission scans, respectively.

The residence times for the upper large intestine (ULI), lower large intestine (LLI), and small intestine were calculated in OLINDA/EXM 1.0 using the ICRP 30 GI model (*18*). The model requires a value for the amount of activity that enters the small intestine. This value was equal to the largest decay-corrected fraction of IA encompassed by the intestinal ROI. The final organ absorbed doses were determined for each subject using the residence times calculated above and were based on the MIRD scheme of a 70 kg adult male (*19*).

RESULTS

Intravenous injection of [^{18}F]SPA-RQ produced no clinically observable effects. Blood pressure, pulse, and respiratory rates showed no significant change from baseline values. In addition, blood and urine tests performed approximately 24 h after the administration of the tracer showed no significant changes from the results obtained at the subjects' initial screening assessments.

The brain, thyroid, lungs, heart, liver, kidneys, intestines, urinary bladder, testes, and red marrow were all identified as source organs on 2-D planar (Figure 1), bisected, and thin-slice image sets. The lungs had the highest uptake of [^{18}F]SPA-RQ with an

average peak activity of 53% IA (n = 7) at about 2 min after injection, measured on the thin-slice data set. The red marrow, liver and kidneys also exhibited relatively high uptake of radioactivity with respective peak values of 9.5%, 9.4% and 8.7% IA, while the brain, heart, thyroid and testes had peak uptakes of 3.4%, 1.0%, 0.3%, and 0.1%, respectively. With the exception of the liver, testes, and red marrow, where uptake reached its peak between 25 and 35 min post-injection, all activity for the above organs peaked within 15 min of the administration of the tracer (Figure 2). The average decay-corrected activity encompassed by the intestinal ROI reached its peak value of 18% IA approximately 30 min post-injection (Figure 3).

The average cumulative urine activity of the seven subjects was fit with a biexponential curve using PRISM (v4.0) software. For some subjects, the program was unable to fit the data. In these cases, a few of the initial data points were excluded, because the activity at these times was minimal and likely highly variable. The asymptote of the biexponential curve fit to the mean urinary activity data determined from the thin-slice images indicated that 41% of the injected activity was excreted via urination (Figure 4). The biological half-lives were 2.9 and 8.3 h. The r^2 value of the bi-exponential curve was 0.999, suggesting a high goodness of fit.

The mean residence times of all source organs from all three analyses, with the exception of the intestines and urinary bladder, are displayed in Table 1. The data suggest the greatest variations in residence times occurred between the thin-slice and 2-D planar image analyses. Additionally, organs that are asymmetrically localized in either the anterior or posterior aspect of the body (specifically the heart, kidneys, testes and thyroid) showed the greatest degree of variance. Since the 2-D planar image compressed

all the organs into a single horizontal plane, the ROIs encompassed activity both anterior and posterior to these localized organs and overestimated uptake and residence times. Because the body was split into anterior and posterior slices for the bisected images, the residence times obtained from this analysis were more similar than the 2-D planar data to the thin-slice values.

The residence time of the red marrow was significantly higher for the thin-slice analysis than for the bisected or 2-D planar methods. As described in Methods, activity in red marrow was determined with a ROI overlying the skull. The horseshoe-shaped ROI drawn on bisected and 2-D planar coronal images only accounted for activity confined to the superior and lateral aspects of the frontoparietal and temporal bones. In contrast, the thin-slice images showed anterior portion of the frontal bone as well as the posterior portion of the parietal and occipital bones. The activity from these regions was then added to that in the horseshoe-shaped region. As a result, the measured uptake of activity and the residence time were higher for the red marrow in the thin-slice image analysis than they were in the other two image sets. Although counterintuitive, the residence times of "remainder of body" residence times were lower for the bisected and 2-D planar images than the thin-slice data. One would expect the source organ activities to be overestimated in the compressed bisected and 2-D planar images. This was, in fact, the case for individual organs. However, the cumulative uptake of activity accounted for in all ROIs for each method of analysis was relatively uniform (varying, on average, 2-4% between the three methods across all time points). Thus, the differences in the calculated uptake of activity in the red marrow in large part account for the variation in the "remainder of body" residence times among the three image sets.

Varying the urine voiding intervals between 0.6, 1.2, 2.4, and 4.8 h resulted in modest changes to the dose of the urinary bladder wall, and the overall EDs at the respective voiding intervals were 27.1, 28.0, 29.5, 30.9 μSv/MBq, respectively. Table 2 displays both the absorbed radiation doses of all pertinent organs and the overall EDs with an assumed urine voiding interval of 2.4 h for all three methods of analysis. The organs with the highest absorbed radiation doses in the thin-slice image analysis were the lungs (81.8 μGy/MBq), ULI wall (78.2 μGy/MBq), small intestine (69.5 μGy/MBq), urinary bladder wall (56.8 μGy/MBq), and kidneys (56.4 μGy/MBq). Similarly, these organs, as well as the thyroid, had the highest absorbed doses in both the bisected and 2-D planar image analyses.

The ratios displayed in Table 2 suggest the organ doses obtained from the bisected and 2-D planar image analyses were most often comparable to those determined from thin-slice image analysis. Organs asymmetrically localized in either the anterior or posterior aspects of the body, showed the greatest variation in doses when comparing the 2-D planar and thin-slice values. Thus, the doses for these organs were always overestimated in the 2-D planar analysis. The ULI wall, small intestine, and LLI wall, along with the red marrow and osteogenic cells, were the only organs with significantly lower radiation doses in the 2-D planar images than in the thin-slice images. The differences in the red marrow and osteogenic cell doses were expected because the ROI of these "organs" underestimated activity in bone in both the bisected and 2-D planar images, as previously described. Doses to the intestines were lower in the bisected and 2-D planar analyses because the images were more highly compressed than the thin-slice

images. Some of the activity in the intestines was probably underestimated and was likely assigned instead to overlapping portions of the kidneys and liver.

DISCUSSION

Whole-body PET imaging with the NK_1 receptor radioligand [^{18}F]SPA-RQ suggested that the ED of the tracer was 29.5 μSv/MBq (109 mrem/mCi) based on careful analysis of thin-slice images. This value is similar for many other ^{18}F labeled PET tracers, suggesting that the radiation risks from doses that are typical injected activities are well within accepted levels for human subjects who will not benefit from participating in research studies. For example, about 340 MBq (9.2 mCi) would be required to produce an ED of 10 mSv (1 rem) in the standard reference man.

Comparison of Methods. If the thin-slice method is viewed as the "gold standard," then the bisected analysis provided more accurate measures of individual organ doses than did the 2-D planar method. For example, doses to asymmetrically located organs (*i.e.*, testes, heart wall, thyroid and kidneys) from the bisected images were more similar than the 2-D planar images to results from the thin-slice analysis. The significance of any of these differences for either method was questionable, however, since the higher values represent more conservative estimates of radiation burden. In contrast, doses to the intestines, red marrow and osteogenic cells were lower for the bisected and 2-D planar methods than for the thin-slice analysis, largely because of unavoidable deficiencies in the way their ROIs were drawn.

Despite the variations in organ doses, the overall estimate of exposure to the entire body was amazingly similar among the three methods. The ED determined from

the bisected images (29.3 µSv/MBq), differed by less than 1% from the thin-slice value (29.5 µSv/MBq). The 2-D planar ED (32.3 µSv/MBq) was approximately 10% higher than the thin-slice value. Thus, the higher, and more conservative, 2-D planar dose appears to be a reasonable strategy to assess the radiation safety. Nevertheless, thin slice analysis may well be justified for a tracer that is highly localized to a small asymmetrically located organ or tumor.

Although not relevant to patient safety, analyses of the compressed bisected and 2-D planar images required considerably less effort than the thin-slice method and took $1/5^{th}$ and $1/10^{th}$ the amount of time, respectively. Alternatively, the use of combined PET/CT images, which were not available at our institution at the time of data acquisition, might allow more accurate identification of source organs and decrease time required for thin-slice image analysis.

Pharmacological Effects. The average injected mass dose of [^{18}F]SPA-RQ was 4.6 nmol (2.1 µg). This dose produced insignificant changes in laboratory tests, blood pressure, pulse, and respiration rate in all subjects. Therefore, [^{18}F]SPA-RQ appears to be safe from both pharmacological and radiation exposure standpoints.

Pulmonary Uptake. Uptake of radioactivity in lungs far exceeded that in any other organ, with a peak value of 53% IA shortly after injection of [^{18}F]SPA-RQ. The lungs of guinea pigs and humans contain high densities of NK_1 receptors that readily bind radioligand antagonists (*21-22*). Thus, a sizeable proportion of the early lung activity probably reflected [^{18}F]SPA-RQ binding to NK_1 receptors, rather than activity in the pulmonary blood volume. Despite the high initial uptake of radioligand, the dose to the lungs (81.8 µGy/MBq) was only moderately higher than other organs because of the fast

washout of activity. Lung activity decreased by about 50% within 30 min of [^{18}F]SPA-RQ injection.

Excretion. With the exception of the lungs, four excretory organs (*i.e.*, ULI wall, small intestine, urinary bladder wall, and kidneys) had the greatest radiation burdens with doses of 78, 70, 57 and 56 μGy/MBq, respectively. The mean, decay-corrected cumulative activity in urine was 41% IA, and that entering the small intestine was 18% IA. Thus excretion of radioactivity from [^{18}F]SPA-RQ via the urine was about twice that of the hepatobiliary route.

Assessment of Risk. Some experts think that a single measure of radiation exposure (*i.e.*, ED) is the best way to assess overall radiation burden and to communicate the corresponding risk to research subjects. For the radioligands listed in Table 3, the EDs showed relatively little variation. For those studies based on human biodistribution data, the ED differed by a factor of 1.5, from 194 to 290 μSv/MBq. Although these values may vary because of true differences in radiation exposure among the ligands, differences in experimental design and data analysis may have caused these variations. If these variations in ED are real, then dosimetry studies like that presented here are useful to assess risk. If these differences merely reflect subtleties in experimental design and analysis, however, then the utility of dosimetry studies for neuroreceptor radioligands is questionable.

Conclusion. Whole-body PET imaging with [^{18}F]SPA-RQ demonstrated a moderate radiation risk profile that would allow a subject to receive multiple injections of the radioligand in a single year. Bisected and 2-D planar images almost always provided more conservative organ dose estimates than thin-slice images, which may actually be

beneficial for patient safety. Coupled with savings in time of image analysis, these conservative dose estimates suggest that either the bisected or 2-D planar method is acceptable to measure human radiation burden for radiotracers with a fairly broad distribution in the body.

ACKNOWLEDGEMENTS

This research was supported by the Intramural Program of NIMH (project #Z01-MH-002852-01). We gratefully acknowledge the staff of the NIH Clinical Center PET Department and Vanessa Cropley, Anil Ramachandran, Masanori Ichise, and Janet Sangare for the successful completion of this study.

REFERENCES

1. Saria A. The tachykinin NK1 receptor in the brain: pharmacology and putative functions. Eur J Pharmacol 1999; 375(1-3):51-60.

2. Pendergrass K, Hargreaves R, Petty KJ, Carides AD, Evans JK, Horgan KJ. Aprepitant: an oral NK1 antagonist for the prevention of nausea and vomiting induced by highly emetogenic chemotherapy. Drugs Today (Barc) 2004; 40(10):853-63.

3. Kramer MS, Cutler N, Feighner J, Shrivastava R, Carman J, Sramek JJ, et al. Distinct mechanism for antidepressant activity by blockade of central substance P receptors. Science 1998; 281(5383):1640-1645.

4. Stockmeier CA, Shi X, Konick L, Overholser JC, Jurjus G, Meltzer HY, et al. Neurokinin-1 receptors are decreased in major depressive disorder. Neuroreport 2002; 13(9):1223-1227.

5. Toru M, Watanabe S, Shibuya H, Nishikawa T, Noda K, Mitsushio H, et al. Neurotransmitters, receptors and neuropeptides in post-mortem brains of chronic schizophrenic patients. Acta Psychiatr Scand 1988; 78(2):121-137.

6. Tooney PA, Crawter VC, Chahl LA. Increased tachykinin NK(1) receptor immunoreactivity in the prefrontal cortex in schizophrenia. Biol Psychiatry 2001; 49(6):523-527.

7. Deguchi K, Antalffy BA, Twohill LJ, Chakraborty S, Glaze DG, Armstrong DD. Substance P immunoreactivity in Rett syndrome. Pediatr Neurol 2000; 22(4):259-266.

8. Rioux L, Joyce JN. Substance P receptors are differentially affected in Parkinson's and Alzheimer's disease. J Neural Transm Park Dis Dement Sect 1993; 6(3):199-210.

9. Fernandez A, de Ceballos ML, Jenner P, Marsden CD. Neurotensin, substance P, delta and mu opioid receptors are decreased in basal ganglia of Parkinson's disease patients. Neuroscience 1994; 61(1):73-79.

10. Quigley BJ Jr, Kowall NW. Substance P-like immunoreactive neurons are depleted in Alzheimer's disease cerebral cortex. Neuroscience 1991; 41(1):41-60.

11. Solin O, Eskola O, Hamill T, Bergman J, Lehikoinen P, Grönroos T, et al. Synthesis of and characterisation of a potent, selective, radiolabeled substance-P antagonist (SPA) for NK_1 receptor quantitation: ([^{18}F]SPA-RQ). Mol Imaging Biol 2004; 6(6):373-384.

12. Hargreaves R. Imaging Substance P receptors (NK1) in the living human brain using Positron Emission Tomography. J Clin Psychiatry 2002; 63 Suppl 11:18-24.

13. Tipre DN, Lu JQ, Fujita M, Ichise M, Vines D, Innis RB. Radiation dosimetry estimates for the PET serotonin transporter probe [^{11}C]DASB determined from whole-body imaging in nonhuman primates. Nucl Med Commun 2004; 25:81–86.

14. Chin FT, Morse CL, and Pike VW. Production of [^{18}F]SPA-RQ as a PET Radioligand for Imaging Human Brain NK_1 Receptors. J Label Compd Radiopharm 2006; 49:17-31.

15. International Commission on Radiation Protection. Report of the Task Group on Reference Man. ICRP Publication 23 (Oxford: Pergamon Press) (1974).

16. Cloutier RJ, Smith SA, Watson EE, Snyder WS, Warner GG. Dose to the fetus from radionuclides in the bladder. Health Phys 1973; 25(2):147-161

17. Stabin MG, Sparks RB, Crowe E. OLINDA/EXM: The Second-Generation Personal Computer Software for Internal Dose Assessment in Nuclear Medicine. J Nucl Med 2005; 46(6):1023-7.

18. International Commission on Radiological Protection. Limits for intakes of radionuclides by workers. ICRP Publication 30 (Oxford: Pergamon Press) (1979).

19. Loevinger R, Budinger TF, Watson EE. MIRD primer for absorbed dose calculations. New York: The Society of Nuclear Medicine; 1991.

20. International Commission on Radiological Protection. Radiological protection and safety in medicine. ICRP Publication 73 (Oxford: Pergamon Press) (1996).

21. McKee KT, Millar L, Rodger IW, Metters KM. Identification of both NK1 and NK2 receptors in guinea-pig airways. Br J Pharmacol 1993; 110(2):693-700.

22. Naline E, Molimard M, Regoli D, Emonds-Alt X, Bellamy JF, Advenier C. Evidence for functional tachykinin NK1 receptors on human isolated small bronchi. Am J Physiol 1996; 271(5 Pt 1):L763-767.

23. Tipre DN, Fujita M, Chin FT, Seneca N, Vines D, Liow JS, et al. Whole-body biodistribution and radiation dosimetry estimates for the PET dopamine transporter probe 18F-FECNT in non-human primates. Nucl Med Commun. 2004; 25(7):737-42.

24. Seneca NB, Schou M, Pauli S, Mozley PD, Liow JS, Sovago J, et al. Whole-body biodistribution, radiation dosimetry estimates for the PET norepinephrine transporter probe [^{18}F]FD_2MeNER in nonhuman primates. Nucl Med Comm. 2005;26(8):695-700.

25. Deloar HM, Fujiwara T, Shidahara M, Nakamura T, Watabe H, Narita Y, et al. Estimation of absorbed dose for 2-[F-18]fluoro-2-deoxy-D-glucose using whole-body positron emission tomography and magnetic resonance imaging. Eur J Nucl Med 1998; 25(6):565-574.

26. Brown WD, Oakes TR, DeJesus OT, Taylor MD, Roberts AD, Nickles RJ, et al. Fluorine-18-fluoro-L-DOPA dosimetry with carbidopa pretreatment. J Nucl Med 1998; 39(11):1884-1891.

27. Bottlaender M, Valette H, Roumenov D, Dolle F, Coulon C, Ottaviani M, et al. Biodistribution and radiation dosimetry of ^{18}F-fluoro-A-85380 in healthy volunteers. J Nucl Med 2003; 44(4):596-601.

28. Goldstein DS, Coronado L, Kopin IJ. 6-[Fluorine-18]fluorodopamine pharmacokinetics and dosimetry in humans. J Nucl Med 1994; 35(6):964-73.

TABLE 1
Mean residence times of identified source organs*

Organ	Residence times (h)		
	Thin Slice	Bisected	2-D Planar
Brain	0.086 ± 0.016	0.091 ± 0.010	0.093 ± 0.011
Heart	0.012 ± 0.002	0.019 ± 0.005	0.049 ± 0.011
Kidneys	0.080 ± 0.008	0.101 ± 0.011	0.141 ± 0.015
Liver	0.193 ± 0.064	0.173 ± 0.042	0.195 ± 0.060
Lungs	0.462 ± 0.106	0.459 ± 0.087	0.450 ± 0.098
Red marrow	0.283 ± 0.064	0.106 ± 0.027	0.093 ± 0.036
Testes	0.003 ± 0.001	0.006 ± 0.001	0.010 ± 0.002
Thyroid	0.003 ± 0.0003	0.004 ± 0.002	0.008 ± 0.002
Remainder of body	0.538 ± 0.072	0.767 ± 0.072	0.742 ± 0.057

* Values are means ± SD among the 7 subjects

TABLE 2
Radiation dose estimates for [^{18}F]SPA-RQ*

	Thin-Slice	Bisected		2-D Planar	
Target Organ	µGy/MBq	µGy/MBq	Ratio to Thin-Slice	µGy/MBq	Ratio to Thin-Slice
Adrenals	12.3	12.3	1.00	13.1	1.06
Brain	15.8	16.5	1.04	16.8	1.06
Breasts	6.3	6.8	1.09	6.9	1.11
Gallbladder Wall	15.7	15.2	0.97	15.2	0.97
LLI Wall	28.9	25.7	0.89	22.6	0.78
Small Intestine	69.5	60.2	0.87	52.0	0.75
Stomach Wall	9.2	9.7	1.05	9.6	1.05
ULI Wall	78.2	67.6	0.86	58.2	0.74
Heart Wall	15.5	19.7	1.28	35.9	2.32
Kidneys	56.4	68.3	1.21	92.0	1.63
Liver	30.2	27.6	0.91	30.4	1.01
Lungs	81.8	81.2	0.99	80.1	0.98
Muscle	6.8	7.3	1.07	7.2	1.05
Ovaries	16.9	15.7	0.93	13.4	0.79
Pancreas	10.9	11.3	1.04	11.8	1.08
Red Marrow	28.1	15.8	0.56	14.8	0.53
Osteogenic Cells	18.2	12.6	0.69	12.0	0.66
Skin	4.1	4.6	1.14	4.6	1.12
Spleen	8.5	9.4	1.10	9.9	1.16
Testes	17.4	30.5	1.76	45.2	2.60
Thymus	7.5	8.2	1.10	8.6	1.15
Thyroid	31.3	41.7	1.33	61.6	1.97
Urinary Bladder Wall	56.8	57.4	1.01	58.4	1.03
Uterus	15.3	14.8	0.97	13.8	0.90
Total Body	10.4	10.3	0.99	10.3	0.99
	µSv/MBq	µSv/MBq	Ratio to Thin Slice	µSv/MBq	Ratio to Thin Slice
Effective dose equivalent	37.6	37.3	0.99	40.6	1.08
Effective dose (ED)	29.5	29.3	0.99	32.3	1.10

* 2.4 h urine voiding interval

TABLE 3
Comparison of the radiation burden of [^{18}F]SPA-RQ with other ^{18}F–labeled radiopharmaceuticals

Radiopharmaceutical	Species studied	Effective dose μSv/MBq	Reference
[^{18}F]FECNT	Rhesus monkeys	21.3	(*23*)
(*S*,*S*)-[^{18}F]FMeNER-D_2	Cynomolgus monkeys	33.2	(*24*)
[^{18}F]FDG	Humans	29.0	(*25*)
[^{18}F]FDOPA	Humans	19.9	(*26*)
[^{18}F]Fluoro-A-85380	Humans	19.4	(*27*)
[^{18}F]Fluorodopamine	Humans	22.5	(*28*)
[^{18}F]SPA-RQ	Humans	29.5	-

FIGURE LEGENDS

Figure 1: An example of a series of compressed whole-body planar PET images for a single healthy subject. The images were obtained 2, 20, 100 and 240 min after intravenous injection of 5.2 ± 0.2 mCi of [^{18}F]SPA-RQ. All four decay-corrected images used the same color scale (bottom of figure).

Figure 2 (a & b): Time-activity curves for visually identifiable organs with both high (a) and low (b) uptake of activity following the injection of [^{18}F]SPA-RQ. Activity data were determined from the analysis of thin-slice images and are expressed without correction for radioactive decay as the mean ± SEM of seven subjects.

Figure 3: Time-activity curve for the region of interest surrounding the intestines following the injection of [^{18}F]SPA-RQ. Activity data were determined from the analysis of thin-slice images and are expressed with correction for radioactive decay as the mean ± SEM of seven subjects.

Figure 4: Cumulative urine excretion of decay-corrected radioactivity following the injection of [^{18}F]SPA-RQ. Data are expressed as the mean ± SEM of seven subjects. The biexponential curve was created with PRISM software (v4.0). The asymptote of the curve shows that about 41% of the injected activity was excreted via the urine.

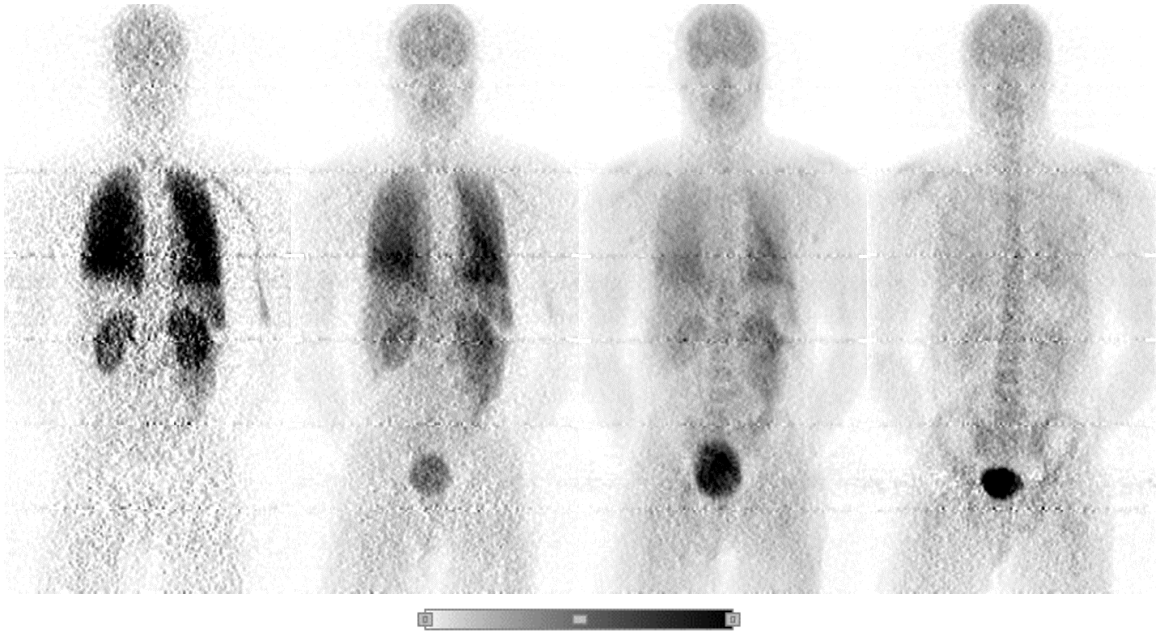

Figure 1

a

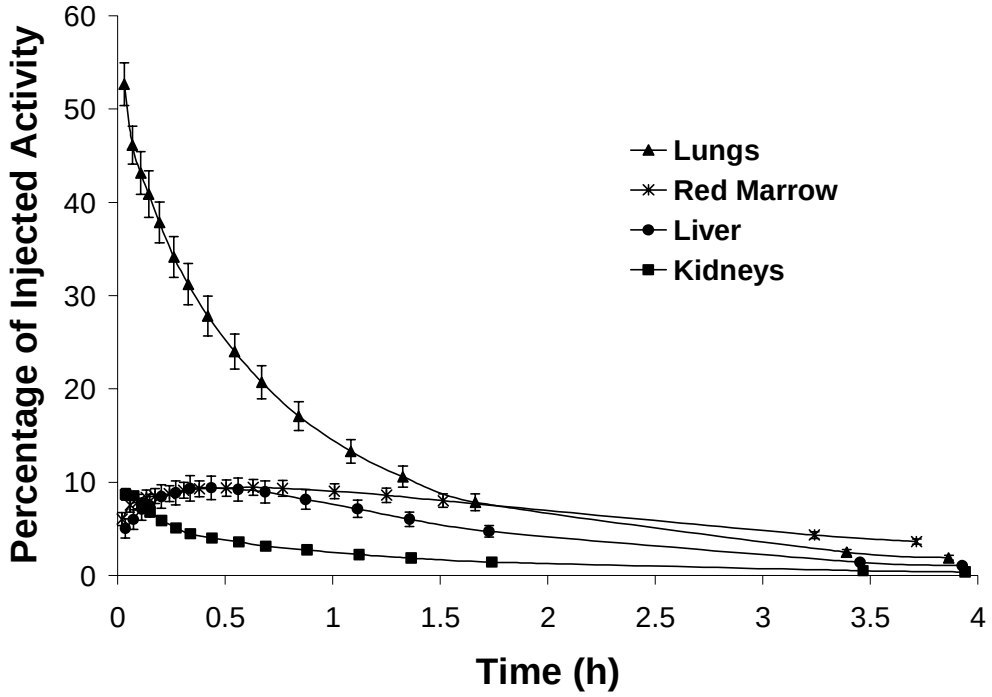
Percentage of Injected Activity
Time (h)
Lungs
Red Marrow
Liver
Kidneys
0
10
20
30
40
50
60
0
0.5
1
1.5
2
2.5
3
3.5
4

b

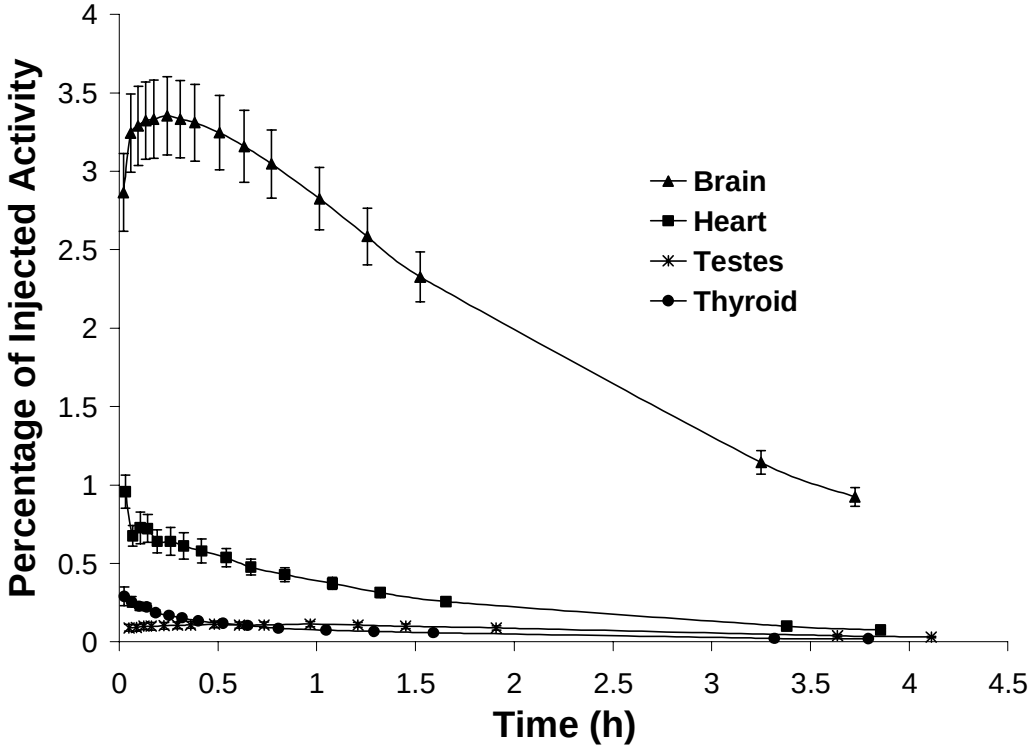
Percentage of Injected Activity
Time (h)
Brain
Heart
Testes
Thyroid
0
0.5
1
1.5
2
2.5
3
3.5
4
0
0.5
1
1.5
2
2.5
3
3.5
4
4.5

Figure 2

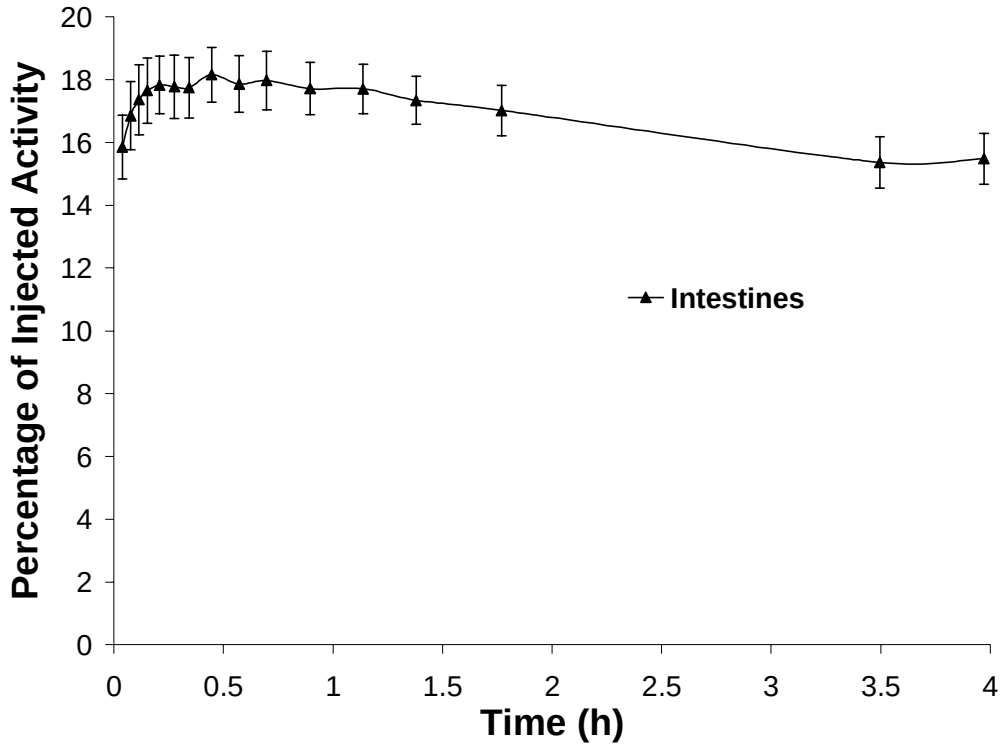

Figure 3

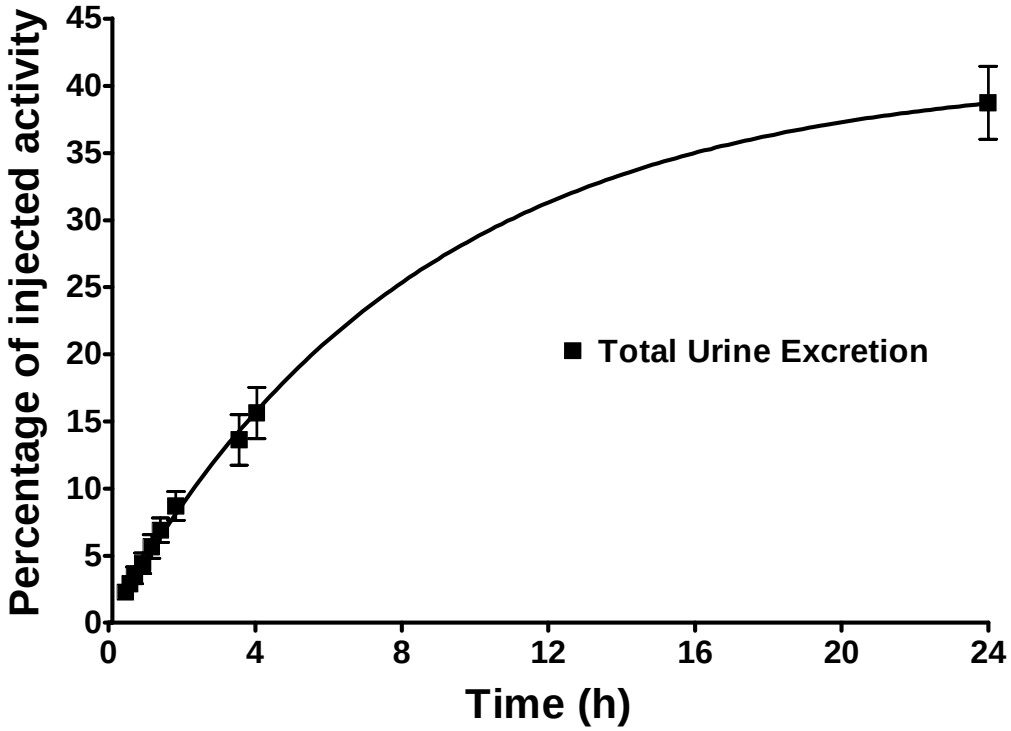

Figure 4

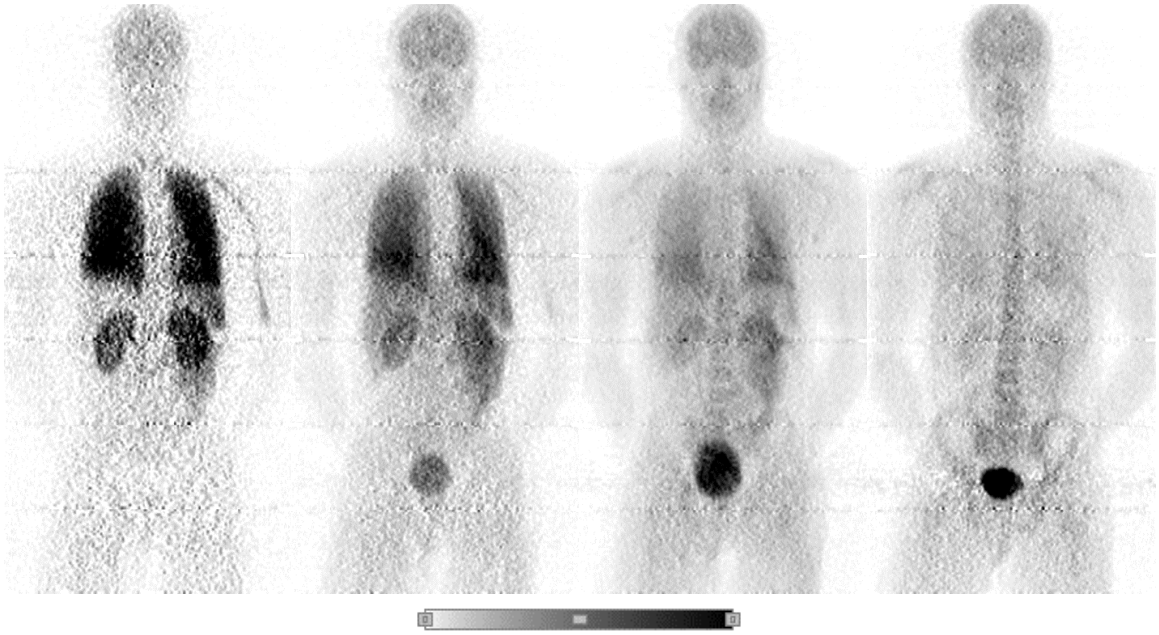

Figure 1

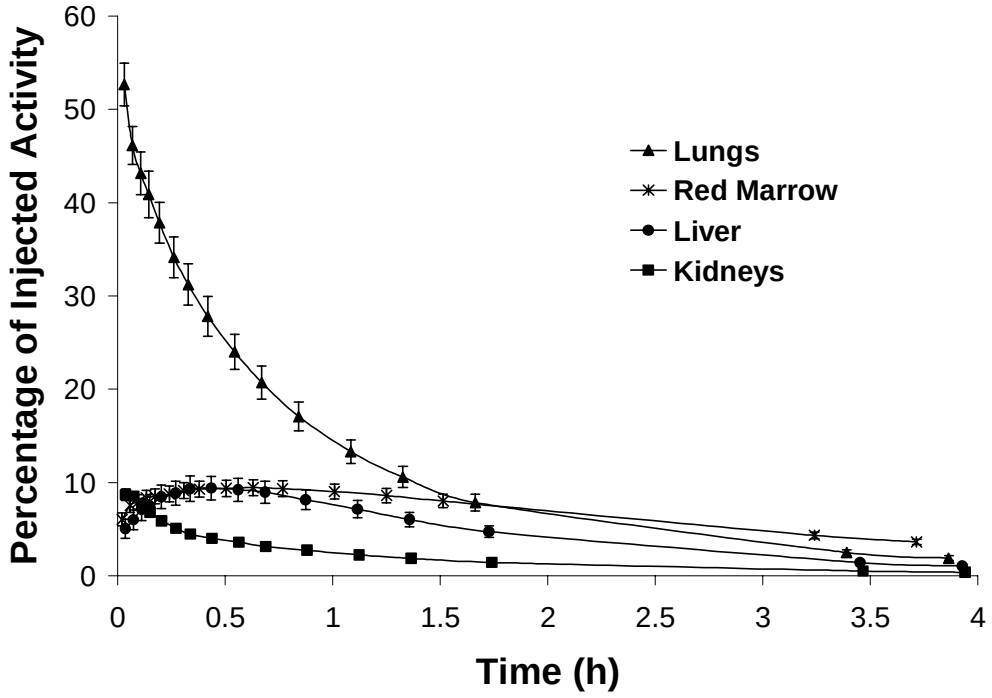

Figure 2(a)

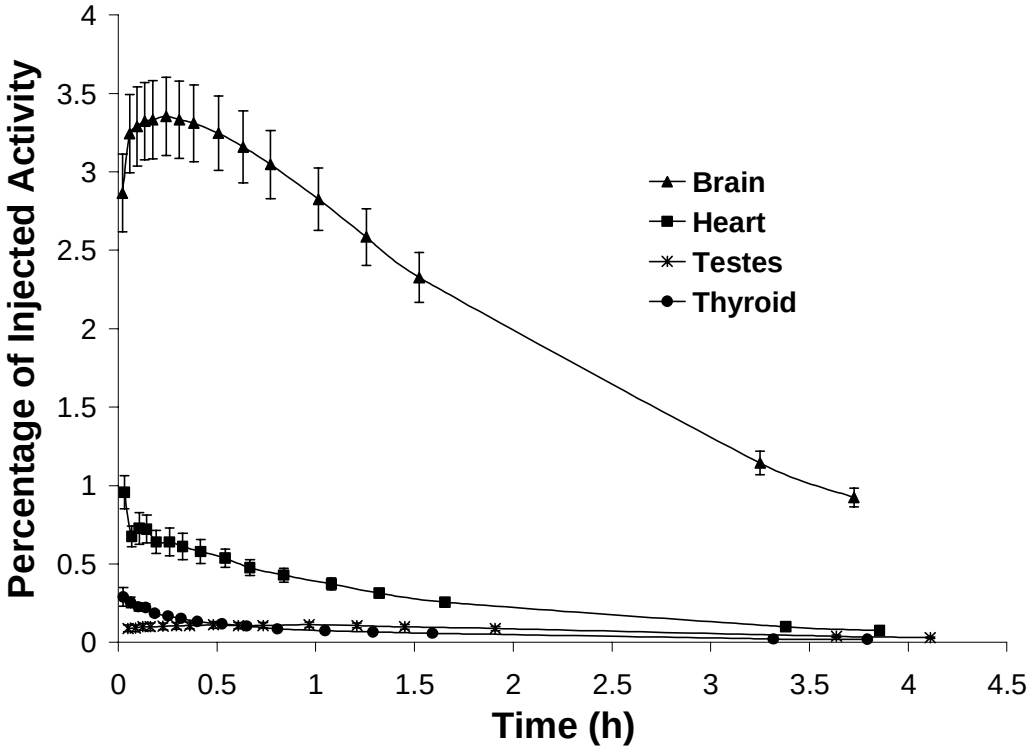

Figure 2(b)

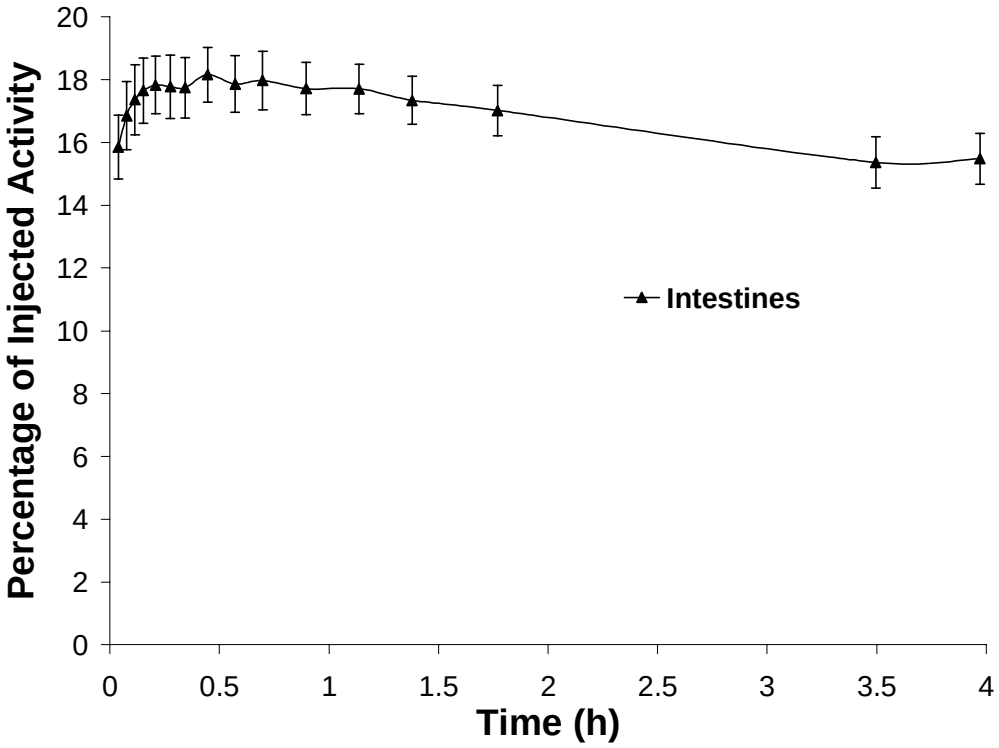
Percentage of Injected Activity
20
18
16
14
12
10
8
6
4
2
0
0
0.5
1
1.5
2
2.5
3
3.5
4
Time (h)
Intestines

Figure 3

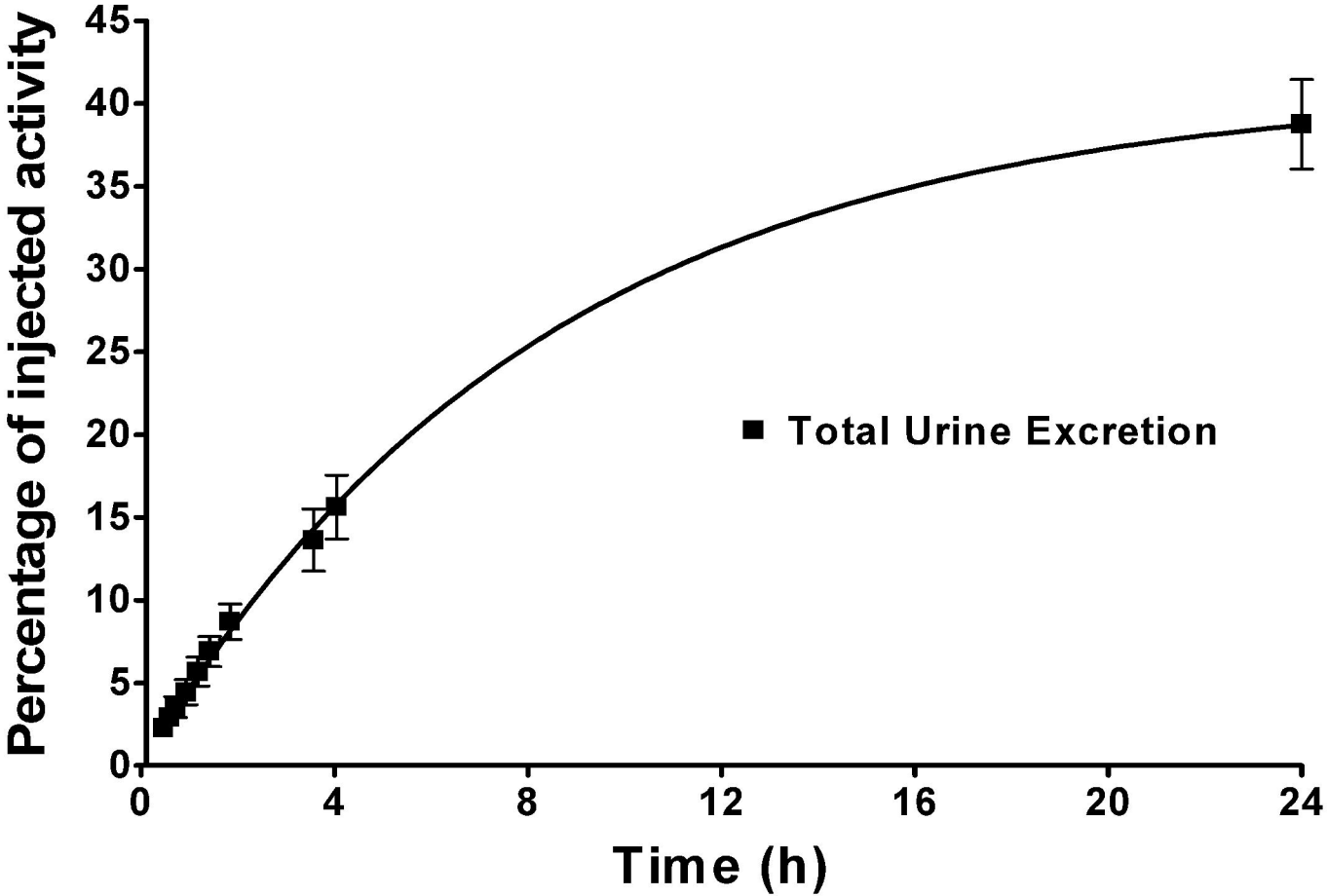
Percentage of injected activity
45
40
35
30
25
20
15
10
5
0
0
4
8
12
16
20
24
Time (h)
Total Urine Excretion